Results in Engineering

A Design Framework for Long-Reach Manipulators in Confined Spaces Using Task-Based Kinematic Optimization and Surface Clustering

--Manuscript Draft--

Manuscript Number:	
Full Title:	A Design Framework for Long-Reach Manipulators in Confined Spaces Using Task-Based Kinematic Optimization and Surface Clustering
Short Title:	
Article Type:	Research paper
Section/Category:	Mechanical Engineering
Keywords:	Kinematic design optimization; Long-reach manipulators; Task Space Clustering; Nuclear fusion maintenance; Confined-space inspection
Corresponding Author:	Emre Uzunoglu UK Atomic Energy Authority Oxford, UNITED KINGDOM OF GREAT BRITAIN AND NORTHERN IRELAND
Corresponding Author Secondary Information:	
Corresponding Author's Institution:	UK Atomic Energy Authority
Corresponding Author's Secondary Institution:	
First Author:	Emre Uzunoglu
First Author Secondary Information:	
Order of Authors:	Emre Uzunoglu
	Dohee Lee
	Luca Raimondi
	Kaiqiang Zhang
	Hongtack Kim
	Youngmin Park
	Kwonhee Hong
	Namil Her
	Robert Skilton
Order of Authors Secondary Information:	
Abstract:	Industrial applications involving hazardous materials often require inspection within confined interiors, posing significant engineering challenges due to restricted access and complex geometries. Long-reach mechatronic systems are essential for these tasks, yet their kinematic design is typically ad hoc. This paper presents a task-driven design synthesis framework to address this gap, focusing on the optimization of manipulators for full-surface inspection inside the vacuum vessel of a nuclear fusion reactor. To facilitate 3D surface service for use in the kinematic optimization pipeline, a methodology is introduced that employs unsupervised surface clustering of CAD-derived geometry. This clustering extracts a compact set of reachability targets while maintaining coverage. Additionally, a lightweight method for 2D plane projection of the clusters enables fast collision pre-checks. Using this reduced task set, a multi-objective NSGA-II simultaneously optimizes kinematic type and dimensions, minimizing total link length and static joint torques, while ensuring position-and-orientation reachability, joint limits, and collision constraints. A representative vessel case study demonstrates that the framework achieves

	collision-free, full-surface coverage through a narrow access port and identifies consistent designs with fewer test points. Surface clustering-based reduction lowers computational costs by up to 60% relative to finer clustering, while maintaining task-space coverage quality. The results demonstrate a systematic and computationally efficient approach to the early-stage design of long-reach manipulators for access-limited environments. Although developed for fusion-vessel inspection, the approach is versatile and can adapt to changes in geometry, constraints, and inspection requirements.
Additional Information:	
Question	**Response**
Results in Engineering is an open access journal which charges an Article Publishing Charge (APC) to cover the cost associated with the publication process. All articles published Open Access will be immediately and permanently free on ScienceDirect for users to read, download, and use in accordance with the author's selected Creative Commons user license. **As an Author, I acknowledge I need to pay the Article Publishing Charge if my manuscript is accepted for publication.**	Yes
To complete your submission you must select a statement which best reflects the availability of your research data/code. IMPORTANT: this statement will be published alongside your article. If you have selected "Other", the explanation text will be published verbatim in your article (online and in the PDF). (If you have not shared data/code and wish to do so, you can still return to Attach Files. Sharing or referencing research data and code helps other researchers to evaluate your findings, and increases trust in your article. Find a list of supported data repositories in Author Resources, including the free-to-use multidisciplinary open Mendeley Data Repository.)	No data was used for the research described in the article.
Free Preprint Service Do you want to share your research early as a preprint? Preprints allow for open access to and citations of your research prior to publication.	NO, I don't want to share my research early and openly as a preprint.

Results in Engineering offers a free service to post your paper on SSRN, an open access research repository, when your paper enters peer review. Once on SSRN, your paper will benefit from early registration with a DOI and early dissemination that facilitates collaboration and early citations. It will be available free to read regardless of the publication decision made by the journal. This will have no effect on the editorial process or outcome with the journal. Please consult the SSRN Terms of Use and FAQs.	

Cover letter

Dr. Emre Uzunoglu
Campus, Culham
Abingdon OX14 3DB
UK Atomic Energy Authority
emre.uzunoglu@ukaea.uk

December 1, 2025

Dear Editor,

Title: A Design Framework for Long-Reach Manipulators in Confined Spaces Using Task-Based Kinematic Optimization and Surface Clustering

Authors: Emre Uzunoglu, Dohee Lee, Luca Raimondi, Kaiqiang Zhang, Hongtack Kim, Youngmin Park, Kwonhee Hong, Namil Her, and Robert Skilton.

We wish to submit an original research article for publication in Results in Engineering. Our work introduces a novel framework and presents results for optimising the kinematic design of long-reach manipulators, tailored for task nuclear maintenance, where inspection must occur within contained confinements through constrained port access. By combining unsupervised surface clustering of dense 3D task geometry with multi-objective optimization, the framework bridges task abstraction and design, enabling efficient, collision-free preliminary kinematic synthesis.

This research presents a novel framework that integrates hybrid geometry-aware surface clustering, PCA-based collision screening, and a multi-objective kinematic optimization pipeline to address the design challenges of long, slender manipulators operating in confined spaces. The method produces a lightweight kinematic optimization process by unsupervised clustering task surfaces and selecting a small set of representative reachability points of the task space. This strategy significantly reduces computational cost while preserving coverage quality and exhibits robust convergence across different clustering resolutions. Although demonstrated on a fusion-vessel inspection scenario, the methodology is general and applicable to a wide range of inspection and maintenance tasks in constrained industrial environments.

We believe that this work closely aligns with the journal's objectives, as it combines theoretical and applied mechanics within practical engineering design to tackle a real-world challenge in robotics, particularly the remote maintenance for nuclear fusion without losing generality. The contribution demonstrates that the introduced methods can offer solutions for the initial stages of robotic design in complex industrial environments with changing task requirements.

We appreciate for your consideration of our work.

Sincerely,
Emre Uzunoglu

Declaration of interests

☒The authors declare that they have no known competing financial interests or personal relationships that could have appeared to influence the work reported in this paper.

☐The authors declare the following financial interests/personal relationships which may be considered as potential competing interests:

Highlights

- Task-based kinematic topology optimisation for fusion-vessel inspection robots.
- Long-reach manipulator kinematic optimisation pipeline for confined task space.
- Unsupervised surface clustering of dense vessel geometry reduces task dimensionality.
- Bridges task abstraction and design for systematic, efficient kinematic synthesis.
- Collision-free coverage; adaptable to vessel shape and evolving operational needs.

A Design Framework for Long-Reach Manipulators in Confined Spaces Using Task-Based Kinematic Optimization and Surface Clustering

Emre Uzunoglu[a,*], Dohee Lee[b], Luca Raimondi[a], Kaiqiang Zhang[a], Hongtack Kim[b], Youngmin Park[b], Kwonhee Hong[b], Namil Her[b], Robert Skilton[a]

[a] *United Kingdom Atomic Energy Authority, Abingdon, OX14 3DB, UK*
[b] *Korea Institute of Fusion Energy, Daejeon, 34133, Republic of Korea*

Abstract

Industrial applications involving hazardous materials often require inspection within confined interiors, posing significant engineering challenges due to restricted access and complex geometries. Long-reach mechatronic systems are essential for these tasks, yet their kinematic design is typically ad hoc. This paper presents a task-driven design synthesis framework to address this gap, focusing on the optimization of manipulators for full-surface inspection inside the vacuum vessel of a nuclear fusion reactor.

To facilitate 3D surface service for use in the kinematic optimization pipeline, a methodology is introduced that employs unsupervised surface clustering of CAD-derived geometry. This clustering extracts a compact set of reachability targets while maintaining coverage. Additionally, a lightweight method for 2D plane projection of the clusters enables fast collision prechecks. Using this reduced task set, a multi-objective NSGA-II simultaneously optimizes kinematic type and dimensions, minimizing total link length and static joint torques, while ensuring position-and-orientation reachability, joint limits, and collision constraints.

A representative vessel case study demonstrates that the framework achieves collision-free, full-surface coverage through a narrow access port and identifies consistent designs with fewer test points. Surface clustering-based re-

*Corresponding author
Email address: emre.uzunoglu@ukaea.uk (Emre Uzunoglu)

duction lowers computational costs by up to 60% relative to finer clustering, while maintaining task-space coverage quality. The results demonstrate a systematic and computationally efficient approach to the early-stage design of long-reach manipulators for access-limited environments. Although developed for fusion-vessel inspection, the approach is versatile and can adapt to changes in geometry, constraints, and inspection requirements.

Keywords: Kinematic design optimization, Long-reach manipulators, Task Space Clustering, Confined-space inspection, Nuclear fusion maintenance

---

1. INTRODUCTION

Engineering applications for inspection and maintenance of interior surfaces in large, confined spaces, such as industrial tanks and vessels with restricted access, pose significant challenges, especially due to hazardous environments. Mechatronic systems, commonly robotic arms, have been widely utilized and developed in industrial practice, as highlighted in [1], with similar challenges related to confined and hazardous environments. Among various service applications in the manufacturing, transportation, and nuclear sectors (see recent advancements in [2, 3, 4] respectively), the fusion reactor vessels are one of the most challenging confined environments due to their limited access ports, complex geometries, and collision-free reachability requirements, all while maintaining the generality of design challenges and solutions.

During the operation of a fusion power plant, plasma is confined within a toroidal vacuum vessel (VV) by strong magnetic fields [5]. Plasma-facing components are exposed to high levels of radiation and high temperatures. These conditions result in the activation and damage of materials and components, necessitating a planned maintenance schedule. Routine maintenance must be carried out as efficiently as possible to maximize plant availability [6]. However, human entry into a fusion VV is prohibited due to hazards such as radiation. Consequently, as in other confined industrial environments containing hazardous materials (e.g., oil refineries, chemical plants), robotic systems are indispensable for performing inspection and maintenance within the VV, a highly constrained space with limited access. Remote service manipulators operating in the VV are exposed to high radiation, high temperatures, and strong magnetic fields, rendering conventional architectures unsuitable. In addition, the VV geometry, with narrow access ports and large workspaces, necessitates long-reach, slender manipulators. Such

designs face significant mechanical challenges, including structural compliance, large joint torque, and reduced stiffness. Representative systems such as the Super Dragon [7], developed for decommissioning tasks, and the Articulated Inspection Arm (AIA) [8] developed by CEA, exemplify the need for bespoke mechatronics and system designs tailored to these constraints.

Despite extensive research on task-based kinematic optimization, including approaches that combine dimensional synthesis, multi-objective optimization, and advanced computational methods, current literature has not addressed the unique requirements of long-reach, slender manipulators operating in confined industrial environments, such as fusion reactors. In [9], a task-oriented dimensional synthesis method is proposed for robotic manipulators with limited mobility, optimizing both geometry and joint variables to minimize pose errors in constrained environments. The study also combines the path planning algorithm and dimensional synthesis to optimize both robot geometry and pose for a set of points. The method was validated on a 4-DoF system for laser operations in aero engines and reported an improved performance in narrow spaces compared to conventional approaches. For another task-oriented case study in a confined environment, [10] developed a steel arch looping manipulator designed for tunnel boring machines. Their method decomposes the manipulator design into modular components using an exponential product model to optimize kinematic and dynamic performance. In [11], a framework is developed for the combined structural and dimensional synthesis of parallel robots, focusing on cryogenic handling tasks. Using multi-objective particle swarm optimization (PSO), they optimized various parallel robot structures' kinematic and dynamic parameters to minimize actuator force and enhance performance in constrained environments.

Recent research in robotic design optimization has explored diverse strategies to improve manipulator performance, adaptability, and workspace. In [12], authors demonstrate how modular robotic architectures can be optimized for automation tasks, highlighting the value of flexible structures that can be tailored to specific operational requirements. In [13], novel local and global performance indices are introduced for workspace optimization, providing quantitative tools to evaluate and improve manipulator reachability and efficiency. In [14], the authors present a biologically inspired approach to design and optimize a monopod robot, emphasizing task-specific mechanical innovations that can improve dynamic performance. Similarly, [15] investigates multi-objective optimization for a hybrid robotic machine tool, inte-

grating performance mapping with trade-off analysis to balance competing design criteria.

In [16], a unified approach is proposed to combine structural and dimensional synthesis, optimizing manipulators with six degrees of freedom (DoF). Their approach incorporates particle swarm optimization to achieve task-specific configurations, demonstrating improved kinematic performance indices during pick-and-place tasks. The use of computational tools has significantly advanced robotic design optimization. For instance, [17] introduces a method that utilizes modular components and a heuristic-guided search to create robots capable of tracking specified motion trajectories.

Although optimizing with a single objective function while combining multiple objectives with pre-assigned weights is possible, multi-objective optimization frameworks have been used to balance competing design goals. In [18], black-box optimization of multiple objectives is adopted to minimize the end effector error while achieving task-specific configurations for assistive robots. In [19], a multi-objective optimization approach is proposed to design a shift manipulator for robot drivers, incorporating both kinematic and dynamic performance evaluations. Their method employs a Simulated Annealing Particle Swarm Algorithm (SA-PSA) to optimize the manipulator's design variables.

Using a kinematic redundancy resolution technique, a multi-objective design optimization approach is proposed in [20] for robotic arms. By introducing virtual joints, they transformed a non-redundant manipulator into a kinematically redundant one, enabling redundancy resolution methods to optimize structural parameters. As a result, the optimization goal is to determine the optimum values of the virtual joints. Their study demonstrates the effectiveness of this method in enhancing manipulability and minimizing condition numbers for surgical robotic applications. In another multi-objective optimization study [21], deep reinforcement learning is used to optimize modular manipulator designs, allowing efficient search and performance evaluation in a high-dimensional design space.

To illustrate how different objective function evaluations impact optimization, [22] presents a methodology for the optimal design of assistive robots comparing three different torque indices. Their approach aimed to minimize joint torque consumption while maximizing the robot's workspace. Using a genetic algorithm, they optimized a 6-DoF wheelchair-mounted robot and demonstrated that each torque index yields distinct design trade-offs between torque efficiency and workspace coverage.

In the context of robot design optimization, the kinematic design of articulated arms for inspection tasks in power plants has not been extensively studied using task-based approaches. Only a few works address applications in nuclear environments, particularly decommissioning. For example, in [23], a mobile platform equipped with two seven-DoF arms is developed, deriving both forward and inverse kinematics to support decommissioning operations in nuclear facilities.

Similarly, in [24], a cable-driven hyper-redundant manipulator (SLIM) is designed to navigate confined industrial environments, aiming to balance reachability and dexterity for inspection task planning. Their study outlines the requirements that guided the design, the main mechanical and electronic subsystems, the control architecture, and results from preliminary experiments with a physical prototype. The 15-DoF robot is capable of positioning its tool centre point within a two-dimensional Cartesian workspace and is designed to operate in harsh environments and high temperatures, achieving a maximum deployment length of approximately 4.8 m.

In [25] the theoretical calculations, kinematic analyses, and structural integrity evaluations for the in-vessel inspection system (IVIS) are presented. The study also explores strategies for design optimization based on these findings and conducts a feasibility assessment to evaluate the suitability of selected technologies for operation under vacuum and high-temperature conditions.

From this analysis, it is clear that kinematic optimization has been extensively investigated in robotics, encompassing dimensional synthesis, multiobjective optimization, and advanced computational methods. However, existing research rarely addresses the distinctive requirements of confined environments, where both reachability and orientation relative to complex surfaces are critical. Most studies assume a fixed set of task poses rather than deriving a compact yet representative task set that guarantees full task-space coverage.

To address this research gap, a new framework is proposed to extract dense task points, comprising positions and surface normals, directly from the vessel geometry. A surface-clustering procedure is then applied to condense these into a reduced set of representative poses, thereby bridging task abstraction and manipulator design while reducing computational cost. Based on this reduced task set, a kinematic optimization process determines the manipulator topology and geometry [26], with the objectives of minimizing the number of degrees of freedom, total manipulator length, and static joint

torques, while ensuring collision-free operation. The framework is inherently adaptable and can accommodate variations in vessel geometry, operational constraints, or evolving inspection and maintenance requirements.

The structure of this study is outlined as follows. Section 2 introduces the details of the use case, workspace environment details, and constraints of the kinematic optimization. Section 3 presents the details of the surface clustering, reachability point selection, optimization algorithm, including objective functions, multi-objective optimization, and algorithm steps. The results are presented in Section 4, in which the best solutions are presented along with the Parent front approach used to obtain the best kinematics configuration. Finally, Section 5 presents conclusions and future work.

2. Problem Statement and Design Constraints

The problem can be summarised as the design of an articulated mechatronic system capable of operating within industrial confinements through constrained access ports. Its kinematic chain must enable the end effector to reach designated operational positions distributed across the interior surface of the confinement. This study adopts the representative environment of the VV of a nuclear fusion reactor as a case study to illustrate the design problem, without loss of generality. Specifically, the design task is defined as identifying an optimized kinematic chain for an articulated robotic arm performing visual inspection within the VV. The robot is intended to inspect the inner surface of the vessel for potential defects after reactor shutdown. Parameters related to visual inspection, such as viewing distance and angle, are treated as fixed specifications rather than optimization variables, allowing flexibility across different use cases and sensor technologies. This assumption is generally valid, because such parameters are typically dictated by the service instrument's design requirements.

Fig. 1 shows the toroidal geometry of the simplified VV considered. The minor radius, r_1, of the VV is set to 4.60 m, the centerline radius, r_2, is 6.80 m, and the major radius, r_3, is 9 m. The total maximum height of the cross section, h, is 8.47 m.

The deployment port, through which the manipulator is inserted inside the VV, is highlighted with a red circle in Fig. 1 and has a radius of 300 mm. When not in use, the robot is stored in a cask outside the deployment port and can access the reactors by actuating a first prismatic joint. To prevent collision with the environment, the revolute joints can be actuated only when

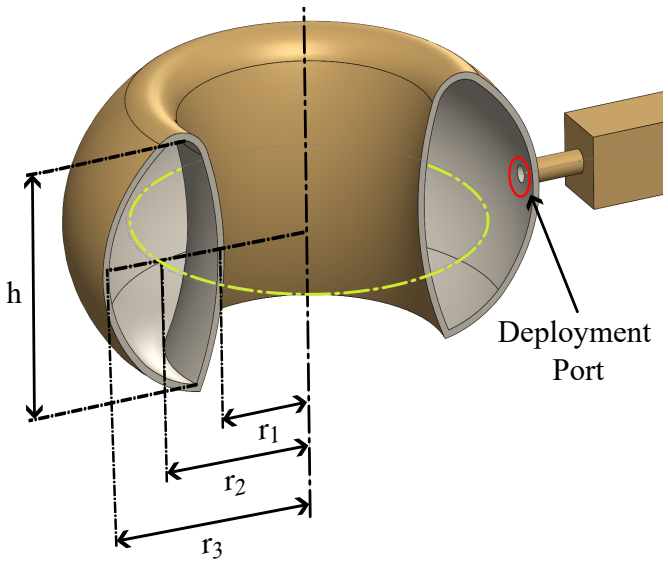

Figure 1: Simplified geometry of the VV (h: height, r_1 minor radius, r_2 center line, r_3 major radius)

0.3 m inside the VV. If any joint remains within the cask, its movement is restricted, and the robot will attempt to reach a position with only the DoF inside the VV.

Fig. 2 shows reachability test points (green markers) and their associated surface normals (red arrows) on the VV first wall, obtained by intersecting the geometry with a section plane. For this case, a multi-DOF robot is visualized inside the VV. The first link (black) acts as a prismatic joint that positions the robot within the vessel. The blue links denote the link dimensions to be optimized, while the purple joints represent the revolute joints treated as kinematic optimization variables.

The problem is to find optimized link lengths and robot joint types to align the tip of the robot with the selected reachability test points and, consequently, design a robot capable of inspecting the surface of the vessel. However, such an optimization would be very costly if all the points on the surface are selected as reachability test points in the optimization process. The challenge of this study is to identify a limited number of reachability test points that ensure sufficient coverage without creating a prohibitively expensive algorithm to optimize the robot's kinematics.

For application-specific optimization of the link length and joint type

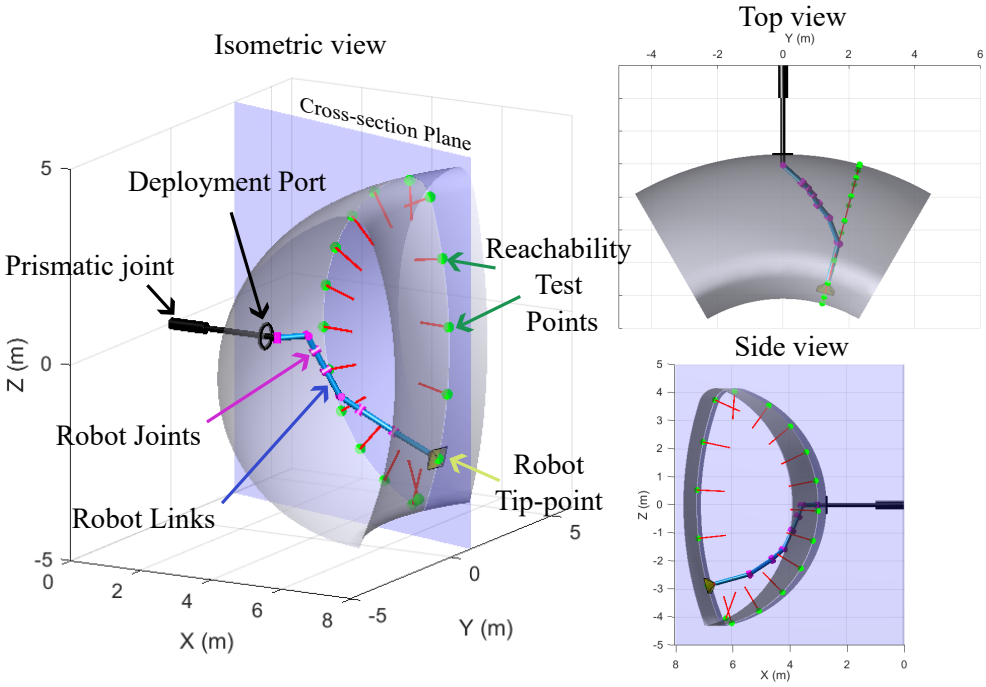

Figure 2: A cross-section of the 3D geometry defined by a blue plane, showing reachability test points (green markers) with normals (red arrows) on the surface. The multi-DOF robot within the VV features a black prismatic joint for positioning, blue links for optimized dimensions, and purple revolute joints for kinematic parameter optimization, illustrated in 3D top and side views.

synthesis, the following constraints are considered:

First Prismatic Joint. The first prismatic joint allows the manipulator to be deployed from the storage cask into the VV. The joint can extend from a position 2.7 m inside the cask, i.e. outside the VV, up to the center line of the VV torus (indicated by the yellow dashed line in Fig. 1), reaching 2.2 m inside the vessel from the entrance port, for a total maximum travel of 4.9 m. Such prismatic mechanisms are commonly adopted to provide sufficient insertion depth for service systems operating within confined industrial environments.

Degrees of Freedom and Joint Types. To ensure reachability in both position and orientation, a minimum of 6 DoF is considered with additional redundant DoFs potentially added during the optimization of the kinematic enumeration (n_{DoF}) to enable avoidance of self-collision and collision with the environment. To simplify the actuation, the robot is designed to have only

revolute joints configured with yaw and pitch, following the first prismatic joint. Throughout the paper, the configurations of the revolute joints will be identified using binary codes; yaw joints will be labeled *1* and pitch joints *0*. For example, a configuration code of *1010* for a 5-DoF robot indicates a sequence of yaw, pitch, yaw, pitch joints following a prismatic joint.

Link Lengths and Joint Limits. The link length l_i $(i = 1, 2, ., n_{DoF})$ is constrained in the range $0.3\ m \leq l_i \leq 1.5\ m$ for ease of deployment and maneuverability inside the VV. Likewise, the rotation range for the revolute joints θ_i is constrained in the range $-90° \leq \theta_i \leq 90°$. In addition, to prevent collision with the entrance port, the revolute joints can initiate motion only after being 0.3 m inside the vessel.

Static Torque Calculation. To calculate the required joint torques under static conditions for a given configuration of the manipulator, a payload of 10 kg at the tip of the last link is considered. This value, as shown in other studies [7, 8], is an estimate in excess of the majority of the end-effector tools, e.g, cameras, used to inspect and maintain fusion reactors. The gravitational contribution of each link is modelled as a linear function of its length, so that longer links will have higher static torque requirements within the optimization. For reference, in a similar system, [27] reports each section (1.2 m in length) having a mass of 6 kg. During optimization, link lengths are updated dynamically, and their corresponding masses are adjusted accordingly.

3. Methodology

The initial part of the methodology presents a new pipeline that reduces the number of reachability test points in kinematic optimization, while preserving the geometric and directional variety of the surface to be examined. This approach aims to accelerate optimization without sacrificing coverage quality, especially in restricted geometries such as the interior of a nuclear fusion vessel. Then, a kinematic optimisation with two objectives, the total link length and the sum of joint torque requirements in static conditions, is introduced to ensure the robot can reach all the target points in position and orientation. For this, the Non-dominated Sorting Genetic Algorithm II (NSGA-II) [28] is employed, which is a widely used multi-objective optimization algorithm that utilizes a crowding distance mechanism to maintain a

diverse set of Pareto-optimal solutions. This method efficiently balances exploration by preserving solution diversity while converging toward the Pareto front.

3.1. Surface Clustering and Reachability Point Selection

Evaluating reachability against every discretized surface point is computationally prohibitive for kinematic optimization in confined geometries. The approach consists of three integrated stages: (i) clustering the surface using a hybrid metric combining position, surface orientation, and distance-to-port; (ii) selecting a globally aware but compact set of representative reachability points per cluster via a diversity-optimized scoring; and (iii) building the PCA-based 2D boundary hulls for fast collision screening. This reduces the number of test points while maintaining coverage of geometric and directional variation relevant to optimization.

The procedure begins with the extraction of points from the mesh file generated from the CAD model. Each extracted point is represented by the following data:

$$\{(\mathbf{p}_i, \mathbf{n}_i, d_i)\}_{i=1}^{N} \tag{1}$$

where $\mathbf{p}_i \in \mathbb{R}^3$ are Cartesian coordinates, $\mathbf{n}_i \in \mathbb{R}^3$ are unit normals, and $d_i \in \mathbb{R}$ is the signed distance to the manipulator entrance port. For a case-specific demonstration, the export mesh file and the surface normals directed towards the operation space of the vessel are extracted from the model represented in Fig. 1.

3.1.1. Hybrid k-means Surface Clustering

Clustering is a fundamental unsupervised learning technique used to partition data into groups based on feature similarity. A popular approach is k-means clustering, which aims to minimize the within-cluster sum of squared distances (variance) to cluster centroids. This method is widely employed because of its relative computational efficiency and conceptual simplicity, especially in large-scale applications like segmentation and vector quantization [29]. Standard k-means uses a unimodal distance metric (typically Euclidean), which limits its applicability when data exhibit multiple features that distinguish them or when similarity cannot be captured by spatial distances alone. In such cases, a hybrid distance metric that combines multiple features can enable more semantically meaningful clusters.

In the methodology, the distance metric is defined as:

$$\Delta_{\text{hyb}}(i,j) = w_{\text{pos}}\Delta_{\text{pos}}(i,j) + w_{\text{ang}}\Delta_{\text{ang}}(i,j) + w_{\text{dist}}\Delta_{\text{dist}}(i,j),$$

where Δ_{pos} is the Euclidean position distance that groups spatially adjacent regions (curvature/extension), Δ_{ang} accounts for the normal vector angular difference which groups similarly oriented patches (tooling/view relevance), and Δ_{dist} refers to differences in signed distance to a reference point which emphasizes accessibility from the entry port with a hybrid distance that balances spatial proximity, local orientation, and accessibility. These terms are defined as follows:

$$\Delta_{\text{pos}}(i,j) = \|\mathbf{p}_i - \mathbf{p}_j\|_2, \tag{2}$$

$$\Delta_{\text{ang}}(i,j) = \arccos(\hat{\mathbf{n}}_i^\top \hat{\mathbf{n}}_j) \tag{3}$$

$$\Delta_{\text{dist}}(i,j) = |d_i - d_j|, \tag{4}$$

$$\tag{5}$$

where w_{pos}, w_{ang}, w_{dist} are empirically chosen weights. Clustering is initialised via $k - means++$ [30] and updated iteratively using the hybrid distance metric. This hybrid metric ensures that clusters are coherent in terms of both spatial proximity and surface orientation, while also grouping points with similar accessibility from the robot base. This weighted combination enables clustering that balances spatial, orientational, and functional relevance, aligning clusters more closely with the kinematic task context. Instead of relying solely on aggregated inertia, the surface normal is encoded with similarity and distance-to-port constraints, thus leveraging rich geometric and task-specific information in the clustering process. In the k-means procedure, each point is assigned to the nearest cluster using the hybrid distance Δ_{hyb}. The centroid of each cluster $\mathcal{C}_m$ is then updated iteratively based on the combined feature vector $[\bar{\mathbf{p}}_m\ \bar{\mathbf{n}}_m\ \bar{d}_m]$.

Fig. 3 shows the outcome of the proposed hybrid k-means surface clustering for three different numbers of clusters. Each color represents a distinct cluster derived from the CAD-based task surface. For each cluster, a local Principal Component Analysis (PCA) is performed on the point coordinates to identify its dominant tangent directions. Specifically, PCA decomposes the local point distribution into orthogonal components: the first and second principal components, span the best-fit tangent plane, while the third

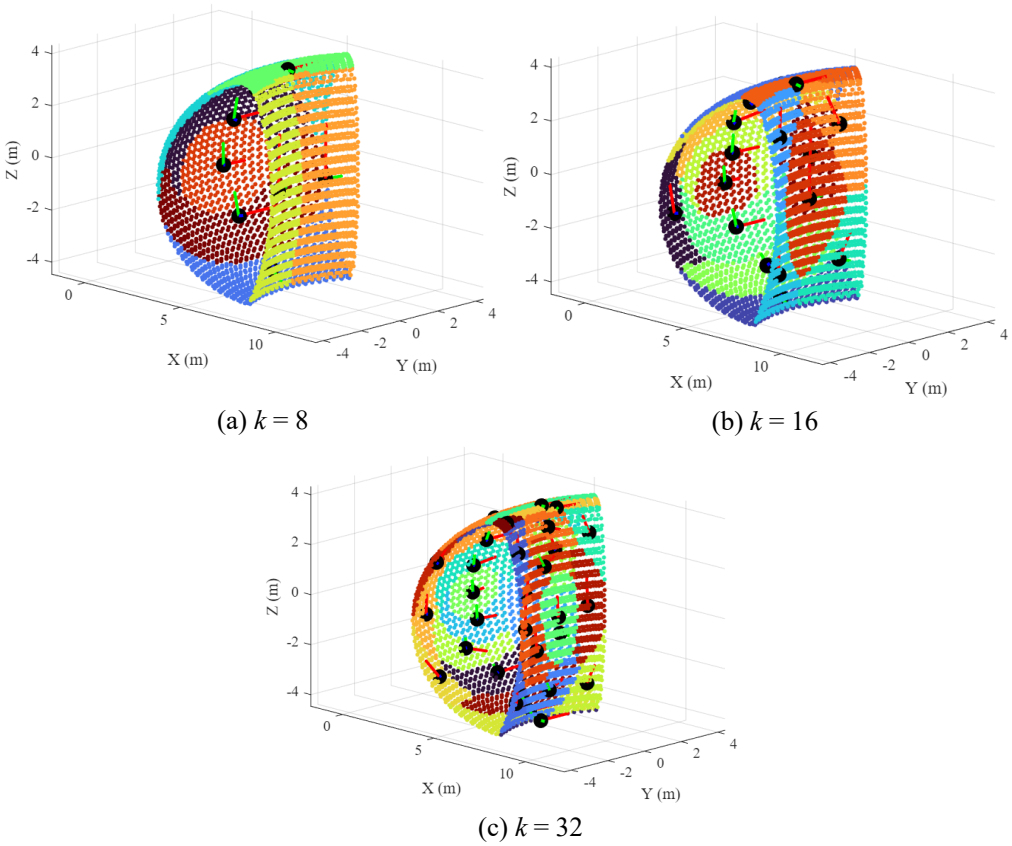

Figure 3: Hybrid clustering results for (a) $k = 8$, (b) $k = 16$, and (c) $k = 32$. Colors denote clusters. Local PCA axes per cluster are overlaid to indicate dominant tangent directions used later for boundary-hull construction.

component corresponds to the surface normal direction (v_1, v_2, v_3). The local PCA axes are overlaid as line segments in the plots to visualise these dominant directions, which are later used to construct the boundart hulls for collision and reachability checks.

3.1.2. Globally Aware Iterative Selection from each Cluster

To ensure that the kinematic optimization is driven by a workspace representation that is both locally accurate and globally comprehensive, a globally aware selection strategy is applied to the clustered task-surface points. While hybrid k-means surface clustering ensures that points within each cluster are spatially coherent, purely local sampling can overlook coverage gaps in the

global workspace. To address this, a selection process that evaluates candidate points not only by their proximity to the cluster centroid but also by their global diversity in position is used.

After the surface clustering is completed, a fixed number of representative points is selected from each cluster for subsequent reachability test point selection. For each cluster, the aim is to have one center and select k test points, ensuring radial extent, global coverage, and directional spread. To ensure cluster diversity, a sequential adjacency-aware selection algorithm is proposed. This approach maintains local diversity by favouring points with distinct radial and angular properties with respect to the cluster center, while introducing a lightweight awareness term that penalises redundancy with recently selected test points in neighbouring clusters.

Let $\mathcal{C}_m = \{\mathbf{p}_{m,i}\}_{i=1}^{N_m}$ denote the set of N_m points in cluster m, and $\bar{\mathbf{p}}_m$ its centroid:

$$\bar{\mathbf{p}}_m = \frac{1}{N_m} \sum_{i=1}^{N_m} \mathbf{p}_{m,i} \tag{6}$$

For each point $\mathbf{p}_{m,i}$ its radial distance is defined from the centroid:

$$r_{m,i} = \|\mathbf{p}_{m,i} - \bar{\mathbf{p}}_m\|_2 \tag{7}$$

and its unit direction vector:

$$\hat{\mathbf{u}}_{m,i} = \frac{\mathbf{p}_{m,i} - \bar{\mathbf{p}}_m}{r_{m,i}}, \quad r_{m,i} > 0 \tag{8}$$

If unit surface normals $\hat{\mathbf{n}}_{m,i}$ are available from the mesh geometry, they are normalized and associated with each point.

The first representative point for each cluster is the medoid, selected by:

$$\arg\min_i \|\mathbf{p}_{m,i} - \bar{\mathbf{p}}_m\|_2 \tag{9}$$

This ensures that the local cluster center is always represented in the reachability test points.

For the choice of the additional k points within each cluster, a scoring function is created:

$$S_{m,i} = \lambda_r R_{m,i} + \lambda_a A_{m,i} - w_p P_{\text{prox}}(m, i) \tag{10}$$

where λ_r and λ_a are the radial and angular weight terms, and w_p adjacency weight penalty.

$$R_{m,i} = \frac{r_{m,i}}{r_m^{90}}, \quad r_m^{90} = \text{percentile}_{90}(\{r_{m,i}\}) \tag{11}$$

Here, r_m^{90} denotes the 90th percentile of radial distances within a cluster, which reflects the typical outer extent of each clusters.

For a candidate with direction $\hat{\mathbf{u}}_{m,i}$ and already-selected local directions $\{\hat{\mathbf{u}}_{m,j}\}$:

$$A_{m,i} = 1 - \max_j \left|\hat{\mathbf{u}}_{m,i}^\top \hat{\mathbf{u}}_{m,j}\right|, \tag{12}$$

This term encourages wide angular separation within the same cluster. In this iterative adjacency penalty addition, only previously processed clusters within an adjacency window L are considered. Let P_{prox} denote the set of representative points selected in the last L clusters, with positions $\mathbf{q}_\ell$ denoting the set of representative points already selected across the clusters up to iteration k, ensuring global awareness during selection.

The penalties are computed as:

$$P_{\text{prox}}(m,i) = \max_k \exp\left[-\left(\frac{\|\mathbf{p}_{m,i} - \mathbf{q}_k\|_2}{\sigma_d\, r_m^{90}}\right)^2\right]. \tag{13}$$

where σ_d can be used to control the decay with distance and angular difference.

Fig. 4 illustrates the reachability points obtained using the procedure proposed for $k = 8$, $k = 16$, and $k = 32$ clusters. In each case, the algorithm selects one central point (located near the cluster centroid $\bar{\mathbf{p}}_m$) and selects 5 points with iterative selection from each cluster that are radially extended and angularly diverse. For lower cluster counts ($k = 8$), the selected points are more widely spaced, producing a coarse but well-distributed coverage of the vessel surface. As k increases to 16 and 32, the point distribution becomes denser and more locally refined, with boundary points capturing finer geometric detail while maintaining global spread through adjacency-aware penalisation.

3.1.3. Collision Plane Generation and Collision Checking in the VV

During the next stage, where the kinematic optimization algorithm is run, collision checking is necessary to ensure the robot configuration can reach the chosen points safely. To perform this efficiently, the clusters previously created are used, and the 3D points are projected onto a 2D planar

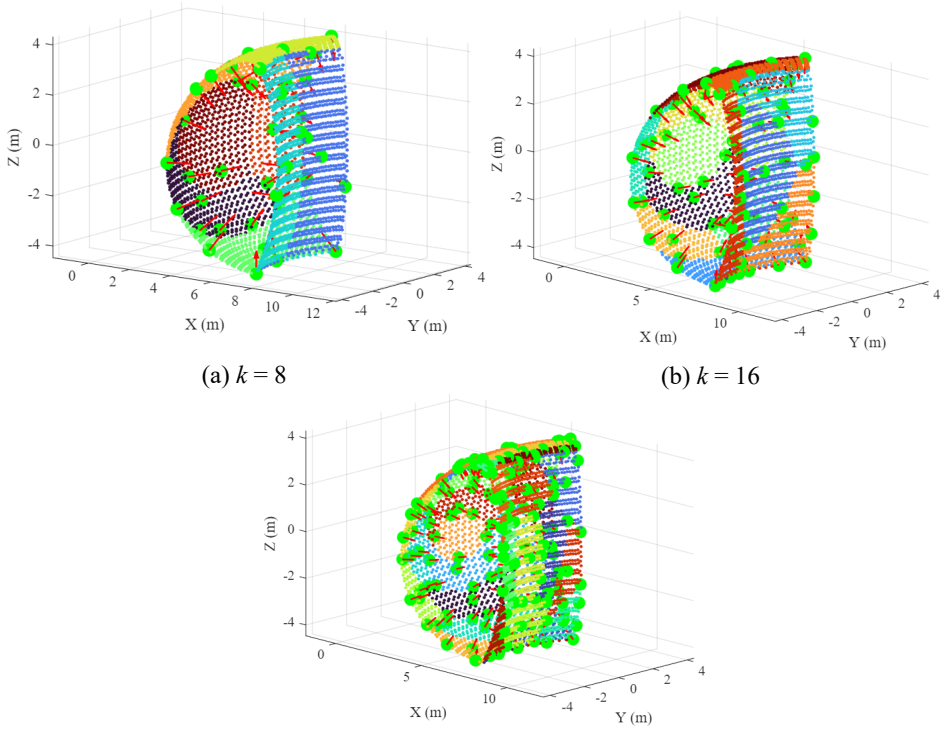

(a) $k = 8$ (b) $k = 16$

(c) $k = 32$

Figure 4: Representative reachability points after globally aware selection. For each cluster: one center (near $\bar{\mathbf{p}}_m$) and 5 points selected with the algorithm for boundary representation. The set is radially extended, globally spread, and angularly diverse, providing a compact but informative test set for optimization.

representation, which enables a fast, approximate check for potential collisions.

For each $\mathcal{C}_m$, PCA on any $\mathbf{p}_i$ yields an orthonormal basis $(\mathbf{v}_1, \mathbf{v}_2, \mathbf{v}_3)$ where $(\mathbf{v}_1, \mathbf{v}_2)$ span the dominant tangent plane and $\mathbf{v}_3$ approximates the local normal. The projected coordinates are:

$$u_i = (\mathbf{p}_i - \bar{\mathbf{p}}_m)^\top \mathbf{v}_1, \quad v_i = (\mathbf{p}_i - \bar{\mathbf{p}}_m)^\top \mathbf{v}_2, \quad w_i = (\mathbf{p}_i - \bar{\mathbf{p}}_m)^\top \mathbf{v}_3. \tag{14}$$

A 2D boundary hull $\mathcal{H}_m$ is computed from (u_i, v_i) to form a conservative guard band $\mathcal{H}_m^+$. A joint position $\mathbf{x} \in \mathbb{R}^3$ is mapped to:

$$u_x = (\mathbf{x} - \bar{\mathbf{p}}_m)^\top \mathbf{v}_1, \quad v_x = (\mathbf{x} - \bar{\mathbf{p}}_m)^\top \mathbf{v}_2, \quad w_x = (\mathbf{x} - \bar{\mathbf{p}}_m)^\top \mathbf{v}_3, \tag{15}$$

In Fig. 5, a representative cluster taken from the processed VV with a hybrid k-means surface clustering algorithm is shown alongside the plane and

the 2D boundary projected onto the plane, which is used for reducing the dimensionality of 3D scattered points.

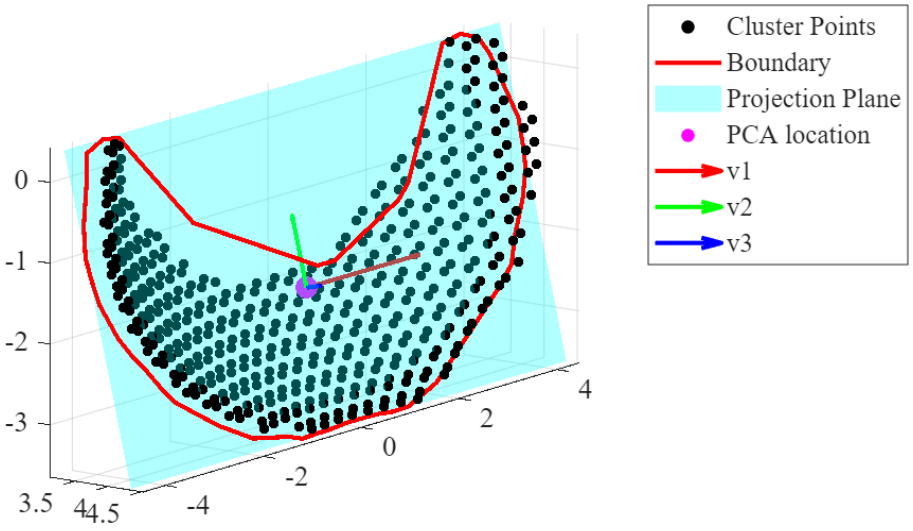

Figure 5: PCA-plane and boundary generated for a representative cluster. Left: projection of cluster points onto $(\mathbf{v}_1, \mathbf{v}_2)$. Right: boundary $\mathcal{H}_m$ and outward expansion $\mathcal{H}_m^+$ used for fast collision screening of joint positions.

Fig. 6 shows the resulting collision surfaces generated for the VV geometry partitioned into 16 clusters. Each cluster and its boundaries are represented with red lines, which show the result of the algorithm to generate the reduced surface representation of each cluster for the VV to be used for collision detection.

An additional rule-based gate is used to check if any joint of the robot inside the vessel is in contact or close to any 2D collision planes. For each joint position in Euclidean space, represented with $\mathbf{q} = [q_x, q_y, q_z]$, the collision of each joint with the surface is checked with Algorithm 1.

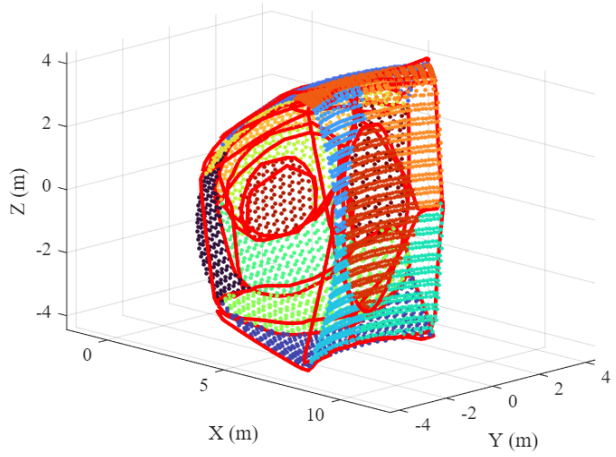

Figure 6: 2D Boundary generated for the k=16 Cluster case

Algorithm 1 PCA-Plane Hull Collision Check for a Joint Position

Require: Joint position $\mathbf{q} \in \mathbb{R}^3$; cluster j data: centroid $\boldsymbol{\mu}'_j$, PCA basis $(\mathbf{v}_1, \mathbf{v}_2, \mathbf{v}_3)$, boundary hull $\mathbf{H}'_j$ of each cluster
Ensure: COLLISION $\in \{\text{true}, \text{false}\}$

Plane distance: $d_\perp \leftarrow \mathbf{v}_3^\top (\mathbf{q} - \boldsymbol{\mu}'_j)$
Projection to plane: $\mathbf{q}_\Pi \leftarrow \mathbf{q} - d_\perp \mathbf{v}_3$
Local 2D coords:
    $u \leftarrow (\mathbf{q}_\Pi - \boldsymbol{\mu}'_j)^\top \mathbf{v}_1, \quad v \leftarrow (\mathbf{q}_\Pi - \boldsymbol{\mu}'_j)^\top \mathbf{v}_2$
Hull inclusion: $h \leftarrow \text{INPOLYGON}\big((u, v), \mathbf{H}'_j\big)$
Decision:
if $|d_\perp| < d_0 \ \wedge \ h = \text{true}$ **then**
    return TRUE {collision}
else
    return FALSE
end if

3.2. Optimization Method

Two objectives, f_1 and f_2, are defined as the cost functions for each candidate solution $\boldsymbol{\xi} \in P$ in the population:

$$f_1 = \sum_{i=1}^{n_{DoF}} l_i, \tag{16}$$

$$f_2 = \frac{1}{m} \sum_{j=1}^{m} \|\boldsymbol{\tau}(j)\|, \tag{17}$$

where f_1 represents the total link length (sum of link lengths l_i), f_2 the average norm of the static joint torque vector $\boldsymbol{\tau}(j)$ evaluated at each configuration $j = 1, \ldots, m$, and m the number of reachability test points used in the optimization.

The two objectives are evaluated together as the objective vector:

$$(f_1, f_2) = FF(\boldsymbol{T_j}, \boldsymbol{\xi}, \boldsymbol{v}), \tag{18}$$

where $\boldsymbol{T_j} \in \mathbb{R}^{4\times4}$ is the homogeneous transformation matrix representing the end-effector pose for task point j, and $\boldsymbol{v}$ denotes design variables such as link lengths and joint types.

The values of candidate solutions $\boldsymbol{\xi}$ generated by the genetic algorithm (GA) represent the kinematic tree and are characterized by $n_{DoF}+1$ parameters:

$$\boldsymbol{\xi} = \left[\xi_1 ... \xi_{n_{DoF}+1}\right] \tag{19}$$

For each candidate solution, the first n_{DoF} parameters are subjected to the constraint defined in equation (20), with lb representing the lower bound and ub representing the upper bound for the link lengths, as detailed in Section 2:

$$lb < \xi_{(1,\ldots,n_{DoF})} < ub \tag{20}$$

The last parameter, $\xi_{n_{DoF}+1}$, uses binary coding. The decimal values ranging from 0 to $2^{n_{DoF}} - 1$ each represent a unique configuration of the kinematic tree, incorporating variations in yaw and pitch joints, as discussed in Section 2. This approach enables the representation of all joint types within the kinematic tree through a single variable.

3.3. Fitness Function Algorithm

Algorithm 2 provides a schematic overview of the optimization workflow to calculate the cost of both objectives for each candidate solution generated by the GA, which focuses on finding the solution for each reachability point and computing the f_1 and f_2. An inverse kinematics solver (IKS) is applied to each generated kinematic structure to test the reachability points and to determine its feasibility for optimization. The IKS employs a weighted

least-squares formulation to minimize task-space errors while accommodating redundancy and complex kinematic structures. This study utilizes the solver to optimize the robot's joint positions while ensuring compliance with design constraints.

The necessary optimization of kinematic enumeration is represented for $n_{DoF} + 1$ variables in vector form by (19). The IKS provides a numerical optimization-based approach to compute joint configurations within the limits. The IKS employs a weighted least-squares formulation to minimize task-space errors while accommodating redundancy and complex kinematic structures. This study utilizes the solver to optimize the robot's joint positions while ensuring compliance with design constraints. Given the desired pose of an end-effector, the inverse kinematics solver computes the joint configurations that realize the desired end-effector pose.

The fitness evaluation function FF is designed to assess the performance of a kinematic structure by determining its ability to reach specified target points while avoiding collisions within a predefined workspace. The algorithm takes as inputs the kinematic parameters ξ, a set of target points T_j, additional variables v related to the kinematic tree configuration, and the geometric model Geo representing the environment.

The process begins with the initialization of the kinematic structure by generating an n-degree-of-freedom (DoF) kinematic tree based on the provided parameters. An initial joint configuration θ_{init} is set, and a tolerance threshold is defined to assess the reachability accuracy. The algorithm then iterates through each reachability test point T_j to find a feasible joint configuration using an IKS. Once a solution $\theta_{\text{sol},i}$ is obtained, the algorithm, referred as CollCheck in 2, checks whether the forward kinematics (FK) solution meets the predefined error tolerance. If the solution falls within the tolerance range, the collision detection step is performed using the algorithm introduced in section 3.1.3 to perform collision checking of each joints position in the 3D space and ensure the joint configuration does not violate environmental constraints. The process is repeated for each joint's position in 3D space. In that case, the initial joint configuration is updated within allowable joint limits, and the process is repeated until a feasible, collision-free solution is found. The algorithm terminates the search for that target point if no viable solution is achieved within a set number of iterations.

In cases where no valid solution is found within the workspace, the algorithm introduces a randomization step to explore alternative joint configurations. If no feasible solution is identified within a limited number of

Algorithm 2 Evaluation of the Fitness Function

Require: ξ , T_j , v , Geo
Ensure: f_1, f_2
Initialization:
Generate n_{DoF} kinematic tree with ξ, v
Set initial joint configuration θ_{init} and reachability error tolerance
$i = 1, ., nDoF$
for $j = 1$ to n_p **do**
  Solve inverse kinematics: $\theta^i_{\text{sol}} \leftarrow \text{IKS}(T_j, \theta_{\text{init}})$
  if $\|T_j - \text{FK}(\theta^i_{\text{sol}})\| \leq$ tolerance **then**
    while CollCheck$(\theta^i_{\text{sol}}, \text{Geo}) ==$ true **do**
      Update θ^i_{init} with joint limits of link exceeding the boundary
      if no feasible solution within limited iterations **then**
        break
      end if
    end while
    if CollCheck$(\theta_{\text{sol},i}, \text{Geo}) ==$ false **then**
      Calculate $\|\tau^i_j\|$ for jth point
    end if
  else
    Attempt randomization for a limited number of steps
    if no feasible solution within operational space **then**
      break
    end if
  end if
end for
Calculate fitness objectives f_1, f_2
Return f_1, f_2

randomization attempts, the process for that specific target point is stopped and the configuration is discarded. When a valid, collision-free solution is successfully identified, the fitness objectives f_1 and f_2 are calculated based on the achieved kinematic performance. Finally, the algorithm returns the computed fitness values, which are used to find the dominant solutions in the genetic algorithm.

4. Results and Discussion

The algorithm is implemented and tested in MATLAB R2024a using the multi-objective NSGA-II function [31], executed for a maximum of 50 generations with a population size of 70, function tolerance is set to 0.005, and maximum stall generations is set to 5 for stopping conditions. These values are selected based on a balance between computational efficiency and solution quality, ensuring sufficient exploration of the search space without sacrificing too much computational cost. The Pareto fraction is set to 0.35, providing a balanced selection of non-dominated solutions. A crossover fraction of 0.8 is applied to promote genetic diversity while maintaining a reasonable convergence speed. As previously described, for each candidate solution, a kinematic tree is generated, and the cost function is evaluated as detailed in Section 3 and with constraints mentioned in Section 2.

A 6-DoF case is initially evaluated to meet the design objectives; however, no feasible solution is obtained because reachability points near the entrance port resulted in collisions with the environment. It is concluded that the manipulator must necessarily accommodate at least a redundant degree of freedom to comply with the shape of the operational space and design constraints. The redundancy also contributes to finding a solution for any reachability point without self-collision and collision with the environment.

The optimization results for the 7 DoF case are presented in Fig. 7. In this figure, the x-axis represents the first objective value, which is the sum of the link lengths, while the y-axis represents the second objective, which is the total torque requirement at all reachable points under static conditions. The blue points indicate all candidate solutions with a valid inverse kinematic solution under the specified constraints, while the green point represents the Pareto front solution obtained with the GA.

In each case, the reachability points are obtained by clustering the CAD-derived surface points and the associated normals as described in Section 2.

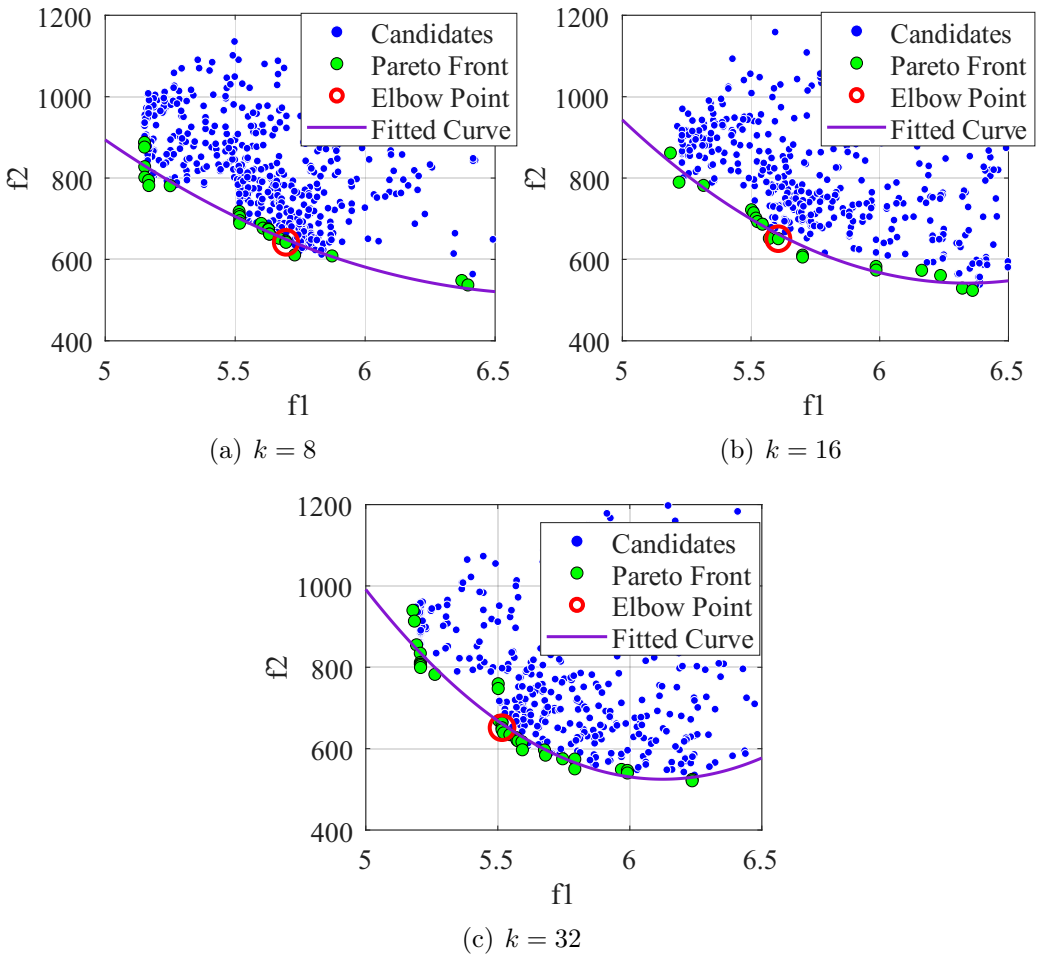

(a) $k = 8$ (b) $k = 16$

(c) $k = 32$

Figure 7: Pareto fronts for $k = 8$, $k = 16$, and $k = 32$ cluster cases, showing the distribution of feasible solutions in the (f_1, f_2) objective space. Red markers indicate the elbow point solution in each case.

In each plot of Fig. 7, the elbow point (trade-off solution) is highlighted, representing a balanced compromise between minimizing f_1 and f_2. This is selected using Chebyshev scalarization method [32], in which each Pareto solution is normalized, and the one minimizing the maximum of the two normalized objectives is chosen [33].

In all three cases, the optimal solutions exhibit proximal placement of yaw joints, which reduces actuator torque requirements by transferring gravitational loads to the manipulator structure instead of the actuators. This

observation is consistent with the trends identified for the 7 DoF configuration results, reinforcing the design principle that proximal yaw joints are beneficial in long-reach manipulators.

In terms of computational cost, the number of clusters directly correlates with the time per generation, as the forward and inverse kinematic checks must be repeated for a larger set of reachability points. However, the added task-space resolution for $k = 16$ and $k = 32$ enables more informed optimization decisions, reducing the likelihood of design candidates failing to reach certain regions. This increase is expected, as each additional cluster adds both local search within the cluster and cross-cluster penalty evaluation steps. While $k = 32$ have the most detailed representation of the vessel surface due to its higher number of test points, it requires approximately 160% more computation time than $k = 8$, providing improved spatial resolution at substantially higher runtime. In contrast, $k = 8$ achieves consistent design patterns at about 38% of the computational cost of $k = 32$. Additionally, $k = 16$ requires approximately 90% more computation time than $k = 8$, offering a balance between fidelity and runtime.

4.1. Comparative Results for $k = 8$, $k = 16$, and $k = 32$

To provide a consistent benchmark across cluster cases, the elbow-point (trade-off) solution from each Pareto front is presented. Table 1 summarises the elbow-point (trade-off) solutions obtained for $k = 8$, $k = 16$, and $k = 32$ clusters. All three elbow-point solutions converge to similar joint-types, reflecting a strong bias towards proximal yaw joints interleaved with distal pitch joints. This structure supports the earlier observation that yaw joints placed proximally reduce actuator torque demands by leveraging gravitational support. Across all cases, the total manipulator length stabilises around 5.5–5.7m, while the static torque requirement remains consistently high (∼640–650Nm). The binary joint-type encodings show that yaw joints (1) dominate the proximal links, with pitch joints (0) used sparingly in the middle of the chain. The similarity of f_1 and f_2 across k indicates that the optimization pipeline converges to structurally consistent designs regardless of the cluster resolution, suggesting robustness of the methodology.

The Pareto fronts for the three clustering levels ($k = 8, 16, 32$) reveal a consistent trade-off between total link length (f_1) and static torque (f_2). In the $k = 8$ case, solutions span the sum of link lengths from approximately 5.15 m up to 6.55 m, with torque values decreasing from nearly 888 Nm to around 486 Nm.

Table 1: Elbow-point (trade-off) solutions across k

k	f_1 (m)	f_2 (Nm)	**Joint Type (binary)**	**Link Lengths (m)**
8	5.70	642.05	1011011	1.2017 0.7887 0.5093 0.8044 0.6234 0.7692 0.9973
16	5.61	650.96	1011011	1.0346 0.5656 0.5974 0.6328 0.7389 0.8157 1.2197
32	5.52	651.52	1011101	0.8516 0.4422 0.5679 0.7770 0.5583 1.0145 1.3037

The distributions of f_1 and f_2 for each cluster size are shown in Fig. 8. The box plots indicate that, while the median link lengths remain close to 5.3–5.6 m across all cluster numbers, the torque distributions are wider for larger k, reflecting the increased difficulty of satisfying more densely sampled workspace constraints. It should also be noted that each clusters have different test points selected.

When evaluating three cluster resolutions, $k = 8, 16, 32$, chosen to double the test points while systematically monitoring convergence, the aim is to identify the smallest k that preserves pose coverage (within position/normal tolerances) and yields a stable Pareto front. Increasing k from 8 to 16 improved task-space coverage and partially refined both the elbow configuration and the spread of Pareto-optimal solutions, as shown in Fig. 7. Moving from 16 to 32 produced only marginal shifts in (f_1, f_2) and did not improve reachability in infeasible regions, while incurring near-linear runtime growth. Therefore, for the selected geometry and tolerances, $k = 8$ provides the fastest scan, while $k = 16$ can be reserved for cases requiring exceptionally fine surface detail and to observe the spread over a large number of test points. On the other hand, $k = 32$ demonstrates that an unnecessarily dense selection of points does not contribute to improving results while increasing the computational cost. This result confirms that the conventional approach of selecting a large number of uniformly sparse test points is unnecessary and often undesired.

The Pareto fronts across the three clustering cases ($k = 8, 16, 32$) reveal clear structural trends linking torque, manipulator length, and joint-type composition.

- **Low-torque, long-length solutions** ($f_2 \approx 166$–178 Nm) consistently require manipulators with total lengths of $f_1 \approx 6.0$–6.4 m. These designs typically incorporate multiple consecutive yaw joints in proximal positions, which provide greater mechanical leverage and reduce static

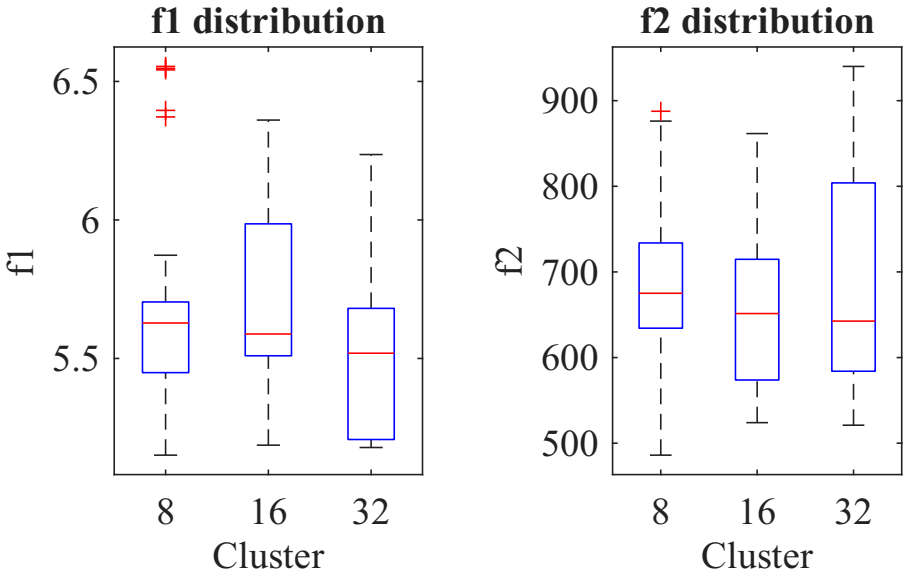

Figure 8: Box plot distributions of optimization results for different numbers of clusters. Left: total link length f_1. Right: total static torque f_2.

torque at the expense of a larger envelope.

- **High-torque, short-length solutions** ($f_1 \approx 5.2$ m, $f_2 \gtrsim 350$ Nm) tend to begin with a pitch joint near the base. While this improves compactness, it increases torque requirements due to reduced ability to counteract gravitational loads through structural leverage.

- **Elbow-point (trade-off) designs** for each k value fall consistently around $f_1 \approx 5.5$–5.7 m and $f_2 \approx 640$–650 Nm. These configurations are characterised by a prismatic insertion joint followed by alternating yaw and pitch joints, where yaw remains dominant in the proximal portion of the chain. This structure balances reachability and torque efficiency, yielding compact yet mechanically feasible manipulators.

Figure 9 illustrates the solution at the elbow point for the $k = 8$ cluster. In the visualisation, yaw joints are shown in yellow and pitch joints in green, while the manipulator tip is represented by a cone indicating the field of view. On the CAD-extracted vessel surface, the designated entrance port is marked by a circle, through which the robot is deployed using the base prismatic actuator.

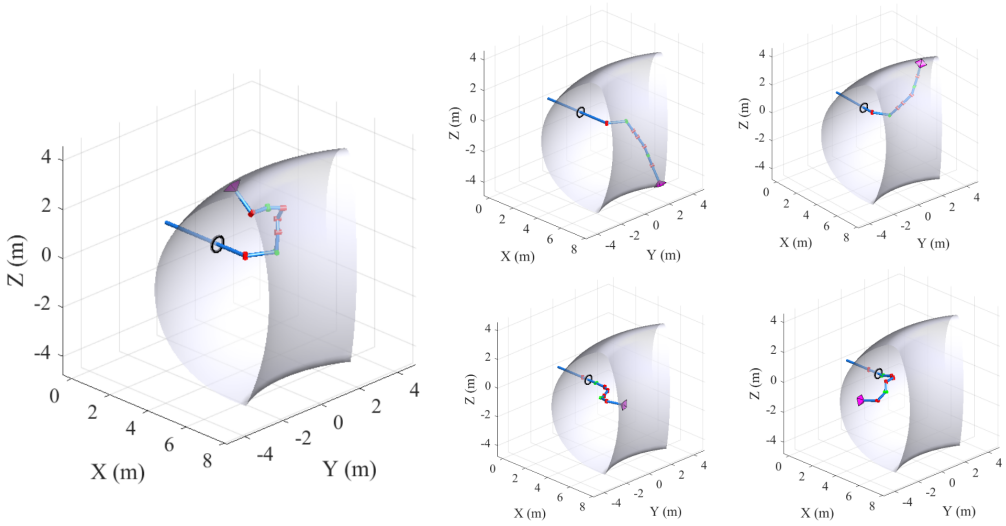

Figure 9: Different configurations for reachability test points of the optimized manipulator given in 1 for k=8 .

To demonstrate that the selected elbow-point solution can cover the task surface without colliding with the vessel, the robot configuration corresponding to the $k = 8$ elbow point is tested for three angular cross-sections of the vacuum vessel (0°, 15°, and 30°). For each cross-section, the inverse kinematics is solved for all associated surface points, and the resulting end-effector poses are plotted. The tip positions are visualised with yellow cones in Fig. 10, showing that the robot can align within tolerance limits for both position and surface normal orientation across all tested sections.

5. Conclusion

This study presented a kinematic optimization framework for long-reach articulated mechatronic systems, i.e., robotic manipulators, specialised for service applications inside industry confinements through port access. The proposed design framework is presented based on the use case of inspection inside a fusion vacuum vessel. The core novelty lies in a hybrid surface-clustering of CAD geometries (combining position, normal, and distance-to-port) with a globally aware selection of a specific number of points, and a lightweight PCA-plane projected collision checking. With these, the kinematic optimization pipeline with NGSA-II is introduced to ensure these com-

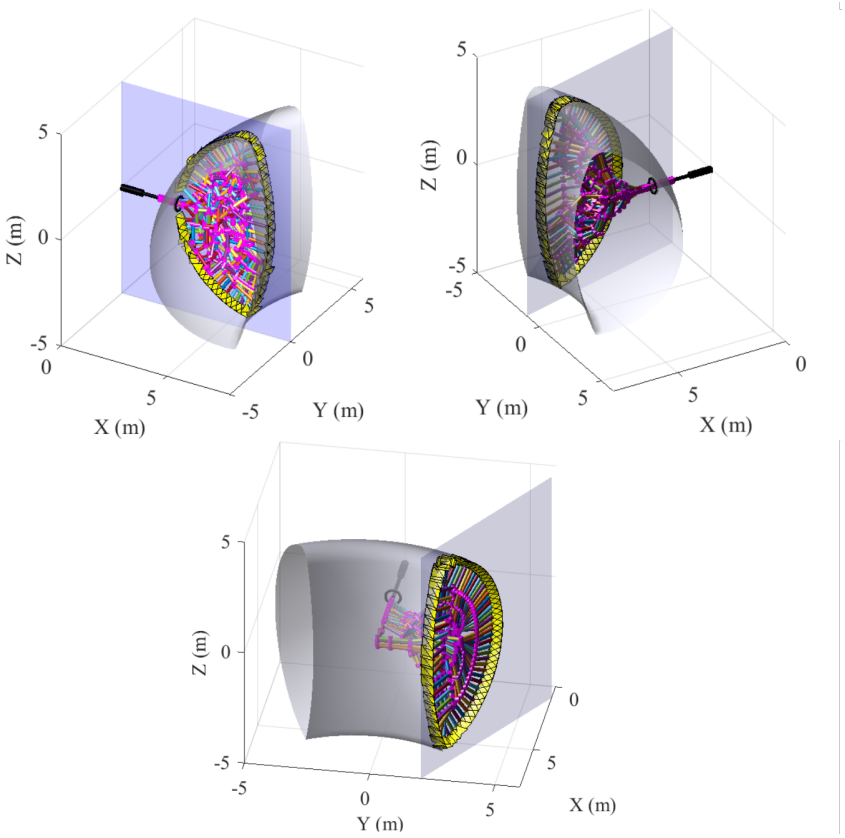

Figure 10: Validation of the $k = 8$ clustered surface elbow-point solution. The robot end-effector is shown for three vessel cross-sections (0°, 15°, 30°). Yellow cones represent feasible tip orientations, demonstrating collision-free coverage within position and normal tolerances.

ponents produce compact, coverage-preserving reachability sets that significantly reduce computational cost while maintaining task fidelity.

On these reduced reachability test points, a multi-objective NSGA-II jointly optimizes kinematic design, minimizing total length and static torque under reachability, orientation, joint limit, and collision constraints. Within $k = 8, 16, 32$ clusters, Pareto–elbow solutions converge to total link lengths of $\sim$5.3–5.7 m and torque f_2 of $\sim$640–650 Nm, with consistent design trends: yaw-dominant proximal joints lower torque, whereas pitch-first chains are more compact but torque-costly.

The clustering results provide a practical guideline. Doubling k from

8→16 improves coverage and refines the elbow only slightly; increasing to $k = 32$ yields only marginal shifts in (f_1, f_2) and no new infeasible regions, while computational costs increase accordingly. Thus, $k = 16$ offers a balanced default for this geometry and tolerances; $k = 8$ is a fast coarse scan. The clustering results provide a practical guideline. Doubling k from 8→16 improves coverage and refines the elbow only slightly; increasing to $k = 32$ yields only marginal shifts in (f_1, f_2) and no new infeasible regions, while computational costs increase accordingly. Thus, $k = 16$ offers a balanced default for this geometry and tolerances; $k = 8$ is a fast coarse scan.

Once Pareto outcomes stabilize with respect to k, the designer can fix the smallest cluster count that preserves coverage and then efficiently explore kinematic constraints (e.g. changing maximum allowed link lengths, inspection tolerances, or viewing distances) at substantially reduced computational cost.

The framework demonstrates that clustering-based task reduction facilitates systematic, early-stage kinematic synthesis for confined environments, while remaining adaptable to changes in vessel geometry, constraints, or inspection requirements.

Future work will integrate structural deflection and actuator limits, and explore hybrid/learning-based optimizers to further improve convergence and robustness.

CRediT authorship contribution statement

Emre Uzunoglu: Conceptualization, Methodology, Software, Validation, Writing – original draft. Dohee Lee: Conceptualization, Investigation, Writing – review & editing. Luca Raimondi: Conceptualization, Investigation, Methodology, Supervision, Writing – original draft. Kaiqiang Zhang: Conceptualisation, Supervision, Methodology, Software, Writing – review & editing. Hongtack Kim: Conceptualization, Investigation. Youngmin Park: Conceptualization, Investigation. Kwonhee Hong: Conceptualization, Investigation. Namil Her: Funding acquisition, Supervision. Robert Skilton: Funding acquisition, Supervision.

Declaration of competing interest

The authors declare that they have no known competing financial interests or personal relationships that could have appeared to influence the work reported in this paper.

Acknowledgements

This work is funded by the UK Department for Science, Innovation and Technology via the International Science Partnerships Fund, and the Republic of Korea's Ministry of Science and ICT under the grant PG2402. The research leading to some outcomes are supported by the UKAEA/EPSRC Fusion Grant 2022/27 EP/W006839/1. The views and opinions expressed herein do not necessarily reflect those of the UK Atomic Energy Authority.

Data availability statement

Data will be made available on request.

References

[1] A. Pistone, D. Ludovico, L. De Mari Casareto Dal Verme, S. Leggieri, C. Canali, D. G. Caldwell, Modelling and control of manipulators for inspection and maintenance in challenging environments: A literature review, Annual Reviews in Control 57 (2024) 100949. doi:10.1016/j.arcontrol.2024.100949.

[2] K. Dandan, A. Ananiev, I. Kalaykov, Siro: The silos surface cleaning robot concept, in: 2013 IEEE International Conference on Mechatronics and Automation, IEEE, 2013, pp. 657–661.

[3] J. Park, D.-h. Kim, J.-w. Seo, D.-c. Lee, S.-h. Kim, G.-w. Chu, J.-s. Woo, S. Han, Design of robotic system for inspection, maintenance and repair of lng cargo tank, in: ISOPE International Ocean and Polar Engineering Conference, ISOPE, 2014, pp. ISOPE–I.

[4] W. Chun, R. Rimando, W. Hamel, Doe robot perspective: Past, present, and future, Nuclear Science and Engineering (2025) 1–19.

[5] I. T. Chapman, N. R. Walkden, An overview of shared technical challenges for magnetic and inertial fusion power plant development, Philosophical Transactions of the Royal Society A 379 (2021) 20200019. doi:10.1098/rsta.2020.0019.

[6] I. T. Chapman, A. W. Morris, UKAEA capabilities to address the challenges on the path to delivering fusion power, Philosophical Transactions of the Royal Society A 377 (2019) 20170436. doi:10.1098/rsta.2017.0436.

[7] G. Endo, A. Horigome, A. Takata, Super Dragon: A 10-m-long coupled tendon-driven articulated manipulator, IEEE Robotics and Automation Letters 4 (2) (2019) 934–941. doi:10.1109/LRA.2019.2894855.

[8] Y. Perrot, others, ITER articulated inspection arm (AIA): R&D progress on vacuum and temperature technology for remote handling, Fusion Engineering and Design 75–79 (2005) 537–541. doi:10.1016/j.fusengdes.2005.06.028.

[9] M. Russo, L. Raimondi, X. Dong, D. Axinte, J. Kell, Task-oriented optimal dimensional synthesis of robotic manipulators with limited mobility, Robotics and Computer-Integrated Manufacturing 69 (2021) 102096. doi:10.1016/j.rcim.2020.102096.

[10] Y. He, M. Yang, Z. Xu, S. Li, B. Zhang, Design of tunnel steel arch looping manipulator with multiple actuators in limited space, Scientific Progress 106 (2023) 00368504231180025. doi:10.1177/00368504231180025.

[11] M. Schappler, P. Jahn, A. Raatz, T. Ortmaier, Combined structural and dimensional synthesis of a parallel robot for cryogenic handling tasks, in: T. Schüppstuhl, K. Tracht, A. Raatz (Eds.), Annals of Scientific Society for Assembly, Handling and Industrial Robotics 2021, Springer, Cham, 2022, pp. 65–77. doi:10.1007/978-3-030-74032-0_6.

[12] S. B. Liu, M. Althoff, Optimizing performance in automation through modular robots, in: Proceedings of the IEEE International Conference on Robotics and Automation (ICRA), 2020, pp. 4044–4050. doi:10.1109/ICRA40945.2020.9197110.

[13] S. Kucuk, Z. Bingul, Robot workspace optimization based on a novel local and global performance indices, in: Proceedings of the IEEE International Symposium on Industrial Electronics (ISIE), Vol. 4, 2005, pp. 1593–1598. doi:10.1109/ISIE.2005.1529155.

[14] S. Xu, F. Li, L. Wang, Y. Fu, Design and optimization of monopod robots for continuous vertical jumping: A novel hopping mechanism inspired by froghoppers and grasshoppers, in: Proceedings of the International Conference on Machine Learning, Pattern Recognition and Automation Engineering, 2024, pp. 41–49.

[15] Z. Gao, D. Zhang, Performance analysis, mapping, and multi-objective optimization of a hybrid robotic machine tool, IEEE Transactions on Industrial Electronics 62 (1) (2014) 423–433. doi:10.1109/TIE.2014.2327583.

[16] D. Ramirez, J. Kotlarski, T. Ortmaier, Combined structural and dimensional synthesis of serial robot manipulators, in: V. Parenti-Castelli, W. Schiehlen (Eds.), ROMANSY 21 - Robot Design, Dynamics and Control, Springer, Cham, 2016, pp. 207–216. doi:10.1007/978-3-319-33714-2_23.

[17] S. Ha, S. Coros, A. Alspach, J. M. Bern, J. Kim, K. Yamane, Computational design of robotic devices from high-level motion specifications, IEEE Transactions on Robotics 34 (5) (2018) 1240–1251. doi:10.1109/TRO.2018.2830419.

[18] K. Kawaharazuka, T. Makabe, K. Okada, M. Inaba, Daily assistive modular robot design based on multi-objective black-box optimization, in: Proceedings of the IEEE/RSJ International Conference on Intelligent Robots and Systems (IROS), 2023, pp. 9970–9977. doi:10.1109/IROS55552.2023.10342041.

[19] G. Chen, X. Xu, L. Wang, W. Zhang, A multi-objective optimization design method of shift manipulator for robot driver using SA-PSA, Structural and Multidisciplinary Optimization 65 (2022) 204. doi:10.1007/s00158-022-03301-1.

[20] O. W. Maaroof, M. I. C. Dede, L. Aydin, A robot arm design optimization method by using a kinematic redundancy resolution technique, Robotics 11 (1) (2022) 1. doi:10.3390/robotics11010001.

[21] J. Whitman, R. Bhirangi, M. Travers, H. Choset, Modular robot design synthesis with deep reinforcement learning, in: Proceedings of the AAAI Conference on Artificial Intelligence, Vol. 34, 2020, pp. 10418–10425, issue: 06. doi:10.1609/aaai.v34i06.6611.

[22] J. D. Sanjuan De Caro, others, Evaluation of objective functions for the optimal design of an assistive robot, Micromachines 13 (12) (2022) 2206. doi:10.3390/mi13122206.

[23] M. J. Bakari, K. M. Zied, D. W. Seward, Development of a multi-arm mobile robot for nuclear decommissioning tasks, International Journal of Advanced Robotic Systems 4 (2007) 51. doi:10.5772/5621.

[24] C. Canali, A. Pistone, D. Ludovico, P. Guardiani, R. Gagliardi, L. De Mari Casareto Dal Verme, others, Design of a novel long-reach cable-driven hyper-redundant snake-like manipulator for inspection and maintenance, Applied Sciences 12 (7) (2022) 3348. doi:10.3390/app12073348.

[25] M. ManoahStephen, others, In-vessel inspection system: Development and testing activities of high vacuum and temperature technologies for fusion remote handling, Fusion Engineering and Design 202 (2024) 114368. doi:10.1016/j.fusengdes.2023.114368.

[26] B. Siciliano, O. Khatib, T. Kröger (Eds.), Springer Handbook of Robotics, Springer, Berlin, 2008.

[27] J. Chalfoun, C. Bidard, D. Keller, Y. Perrot, G. Piolain, Design and flexible modeling of a long reach articulated carrier for inspection, in: 2007 IEEE/RSJ International Conference on Intelligent Robots and Systems (IROS), IEEE, 2007, pp. 4013–4019.

[28] K. Deb, A. Pratap, S. Agarwal, T. Meyarivan, A fast and elitist multiobjective genetic algorithm: NSGA-II, IEEE Transactions on Evolutionary Computation 6 (2) (2002) 182–197. doi:10.1109/4235.996017.

[29] A. M. Ikotun, A. E. Ezugwu, L. Abualigah, B. Abuhaija, J. Heming, others, K-means clustering algorithms: A comprehensive review, variants analysis, and advances in the era of big data, Information Sciences 622 (2023) 178–210. doi:10.1016/j.ins.2022.11.139.

[30] D. Arthur, S. Vassilvitskii, K-means++: The Advantages of Careful Seeding, in: Proceedings of the Eighteenth Annual ACM-SIAM Symposium on Discrete Algorithms (SODA), SIAM, 2007, pp. 1027–1035.

[31] MathWorks, gamultiobj — multiobjective genetic algorithm, accessed 22 September 2025 (2025).
URL `https://www.mathworks.com/help/gads/gamultiobj.html`

[32] S. Wei, M. Niethammer, The fairness–accuracy pareto front, Statistical Analysis and Data Mining: The ASA Data Science Journal 15 (3) (2022) 287–302. doi:10.1002/sam.11560.

[33] I. Giagkiozis, P. J. Fleming, Methods for multi-objective optimization: An analysis, in: 2015 IEEE Conference on Systems, Man, and Cybernetics (SMC), IEEE, 2015, pp. 2820–2827.

Click here to access/download

Supplementary Material (Clean Version - Appears online exactly as provided here)

Video_Abstract.mp4